ASASSN-18ey: The Rise of a New Black Hole X-Ray Binary

M. A. Tucker[1] , B. J. Shappee[1], T. W.-S. Holoien[2,16], K. Auchettl[3,4,5] ,
J. Strader[6] , K. Z. Stanek[3,7], C. S. Kochanek[3,7] , A. Bahramian[6,8]

ASAS-SN,

and

Subo Dong[9], J. L. Prieto[10,11], J. Shields[7], Todd A. Thompson[3,7], John F. Beacom[3,4,7] , L. Chomiuk[6]

ATLAS,

L. Denneau[1], H. Flewelling[1] , A. N. Heinze[1] , K. W. Smith[12], B. Stalder[13] , J. L. Tonry[1],
H. Weiland[1], A. Rest[14], M. E. Huber[1] , D. M. Rowan[1,15] , and K. Dage[6]

[1] Institute for Astronomy, University of Hawai'i, 2680 Woodlawn Drive, Honolulu, HI 96822, USA; tuckerma@hawaii.edu
[2] The Observatories of the Carnegie Institution for Science, 813 Santa Barbara Street, Pasadena, CA 91101, USA
[3] Center for Cosmology and AstroParticle Physics (CCAPP), The Ohio State University, 191 W. Woodruff Avenue, Columbus, OH 43210, USA
[4] Department of Physics, The Ohio State University, 191 W. Woodruff Avenue, Columbus, OH 43210, USA
[5] Dark Cosmology Centre, Niels Bohr Institute, University of Copenhagen, Blegdamsvej 17, DK-2100 Copenhagen, Denmark
[6] Department of Physics and Astronomy, Michigan State University, 567 Wilson Road, East Lansing, MI 48824, USA
[7] Department of Astronomy, The Ohio State University, 140 West 18th Avenue, Columbus, OH 43210, USA
[8] International Centre for Radio Astronomy Research Curtin University, GPO Box U1987, Perth, WA 6845, Australia
[9] Kavli Institute for Astronomy and Astrophysics, Peking University, Yi He Yuan Road 5, Hai Dian District, Beijing 100871, People's Republic of China
[10] Núcleo de Astronomía de la Facultad de Ingeniería y Ciencias, Universidad Diego Portales, Av. Ejército 441, Santiago, Chile
[11] Millennium Institute of Astrophysics, Santiago, Chile
[12] Astrophysics Research Centre, School of Mathematics and Physics, Queens University Belfast, Belfast BT7 1NN, UK
[13] LSST, 950 North Cherry Avenue, Tucson, AZ 85719, USA
[14] Space Telescope Science Institute, 3700 San Martin Drive, Baltimore, MD 21218, USA
[15] Department of Physics and Astronomy, Haverford College, 370 Lancaster Avenue, Haverford, PA 19041, USA

Abstract

We present the discovery of ASASSN-18ey (MAXI J1820+070), a new black hole low-mass X-ray binary (LMXB) discovered by the All-Sky Automated Survey for SuperNovae (ASAS-SN). A week after ASAS-SN discovered ASASSN-18ey as an optical transient, it was detected as an X-ray transient by MAXI/GCS. Here, we analyze ASAS-SN and Asteroid Terrestrial-impact Last Alert System pre-outburst optical light curves, finding evidence of intrinsic variability for several years prior to the outburst. While there was no long-term rise leading to the outburst, as has been seen in several other systems, the start of the outburst in the optical preceded that in the X-rays by 7.20 ± 0.97 days. We analyze the spectroscopic evolution of ASASSN-18ey from pre-maximum to >100 days post-maximum. The spectra of ASASSN-18ey exhibit broad, asymmetric, double-peaked Hα emission. The Bowen blend ($\lambda \approx 4650$ Å) in the post-maximum spectra shows highly variable double-peaked profiles, likely arising from irradiation of the companion by the accretion disk, typical of low-mass X-ray binaries. The optical and X-ray luminosities of ASASSN-18ey are consistent with black hole low-mass X-ray binaries, both in outburst and quiescence.

Key words: accretion, accretion disks – stars: black holes – X-rays: binaries

1. Introduction

Low-mass X-ray binaries (LMXBs) consist of compact objects, either a neutron star (NS) or a black hole (BH), accreting material from a donor star with a typical mass of $M_{\mathrm{donor}} \lesssim 1 M_\odot$. The compact object is surrounded by an accretion disk fed by a donor star undergoing Roche Lobe overflow (RLOF). Observationally, LMXBs can be classified as either transient/outbursting sources or persistent/non-outbursting sources, with the caveat that transient LMXBs can go undetected for years or decades while in quiescence since their X-ray luminosity is low ($L_X \sim 10^{32}$ erg s^{-1}). During an outburst, these systems increase by several orders of magnitude in both X-ray and optical luminosity, routinely leading to their discovery. Conversely, persistent X-ray binaries have higher continuous X-ray luminosities ($L_X \sim 10^{36-38}$ erg s^{-1}), and the

majority of these sources have been discovered by all-sky X-ray surveys.

Transient LMXBs can be grouped into one of three categories based on their X-ray spectral state: high/soft/thermal, low/hard, and very high/steep power law (see Remillard McClintock 2006, for an overview of BH LMXB X-ray properties). The high/soft state is dominated by thermal disk emission, with little to no power-law component. Conversely, the low/hard state is dominated by the power-law emission, contributing $\gtrsim 80\%$ of the observed flux. Finally, the very high state is characterized by a steep power law ($\Gamma > 2$) and usually dominates the X-ray spectra when BH LMXBs approach the Eddington limit. Throughout a single outburst, an LMXB usually experiences at least two of these states as the accretion rate onto the compact object evolves with time.

These transient LMXB outbursts are likely driven by thermal and viscous instabilities in the accretion disk (Dubus et al. 2001; Lasota 2001). Both NS and BH LMXBs can be transient sources, although their outbursts are quantitatively

---

different (see Done et al. 2007 for a review). NS LMXBs generally host smaller accretion disks than their BH counterparts due to tidal truncation by the donor and the lower mass of the compact object. The smaller accretion disk is less likely to be unstable for a given donor star, and even when unstable, these smaller disks result in lower amplitude outbursts than those seen in BH LMXBs (Done et al. 2007). BH LMXBs can exhibit optical outbursts of $\gtrsim 5$ mag (Corral-Santana et al. 2016), and go years between consecutive outbursts (e.g., Russell et al. 2018). These outbursting LMXBs are well described by the classical disk instability model (DIM) with modifications to account for self-irradiation (DIM+irradiation; Dubus et al. 2001).

ASASSN-18ey was discovered by the All-Sky Automated Survey for SuperNovae (ASAS-SN; see Shappee et al. 2014 and Kochanek et al. 2017 for details on cameras, filters, and zero-points) on UT 2018 March 06.58 (MJD 58184.079861) at R.A. $= 18^{\rm h}20^{\rm m}21\overset{\rm s}{.}9$ decl. $= +07°11'07\overset{''}{.}3$ (J2000) with a V-band magnitude of 14.88. It was publicly released within hours of discovery.[17] The source was undetected ($V > 16.7$ mag) on UT 2018 March 02.59, roughly four days prior. Because of its coincidence with a $G = 17.8$ mag $Gaia$ source (ID 4477902563164690816; Gaia Collaboration et al. 2016), ASASSN-18ey was initially labeled as a cataclysmic variable (CV) candidate. Then, six days later on 2018 March 11, the Monitor of All-sky X-ray Image (MAXI; Matsuoka et al. 2009) Gas Slit Camera (Mihara et al. 2011) nova alert system detected a bright X-ray transient at the same location (MAXI J1820 +070, 32 ± 9 mCrab, 4–10 keV; Kawamuro et al. 2018; Denisenko 2018).

Several teams carried out follow-up observations after the MAXI transient alert due to the intrinsic brightness and unknown nature of ASASSN-18ey. Follow-up X-ray observations of ASASSN-18ey were conducted with NICER (Homan et al. 2018a, 2018c; Uttley et al. 2018), $INTEGRAL$ (Bozzo et al. 2018; Kuulkers et al. 2018; Mereminskiy et al. 2018), and XRT/BAT (Buisson et al. 2018; Del Santo & Segreto 2018; Kennea et al. 2018). The first suggestion of ASASSN-18ey being a BH LMXB and the detection of a possible state transition were posted by Baglio et al. (2018) and Homan et al. (2018b), respectively. Optical spectra showed signatures typically associated with LMXBs in outburst including He I and He II in emission combined with an evolving Hα emission profile (Bahramian et al. 2018; Floers et al. 2018; Garnavich & Littlefield 2018; Munoz-Darias et al. 2018). Subsequent optical observations revealed an optical period of $\sim$3.4 hr (Richmond 2018), correlations between X-ray and optical brightness (Paice et al. 2018; Townsend et al. 2018; Yu et al. 2018a), linear polarization (Berdyugin et al. 2018), and (sub-)second flaring (Fiori et al. 2018; Gandhi et al. 2018; Littlefield 2018; Sako et al. 2018; Yu et al. 2018a, 2018b; Zampieri et al. 2018). These rapid photometric variations were confirmed in the near-infrared by Casella et al. (2018), and a large infrared excess compared to archival 2MASS data was noted by Mandal et al. (2018) and Yamanaka et al. (2018). Radio observations may have detected a forming jet and its ensuing quenching (Bright et al. 2018a, 2018b; Broderick et al. 2018a, 2018b; Polisensky et al. 2018; Tetarenko et al. 2018a, 2018b; Trushkin et al. 2018a, 2018b).

Using the $Gaia$ DR2 parallax (Gaia Collaboration et al. 2016, 2018; Luri et al. 2018) and Bailer-Jones et al. (2018) distance priors, ASASSN-18ey is located at a distance of $d = 3.06^{+1.54}_{-0.82}$ kpc, with a total reddening of $E(B - V) = 0.197$ mag (Schlafly & Finkbeiner 2011), corresponding to $A_V = 0.614$ mag assuming $R_V = 3.1$. We discuss pre-outburst data in Section 2, analyze the rising light curves in Section 3, and qualitatively examine the pre- and post-maximum spectra in Section 4. Finally, in Section 5, we discuss our conclusion that ASASSN-18ey is likely a new BH LMXB in outburst.

2. Quiescence

Using archival photometry, we place limits on the maximum mass of the donor star in ASASSN-18ey. We obtain $grizy$ magnitudes from the Pan-STARRS (PS) Stack Object Catalog[18] (SOC; Chambers et al. 2016; Flewelling et al. 2016) and compare them to the absolute magnitudes from the PARSEC[19] (Marigo et al. 2017) stellar isochrones. There are two entries in the PS SOC for ASASSN-18ey, so we take the entry with the brighter r-band magnitude, although they are comparable in all filters. The source does not appear extended or blended in the Pan-STARRS catalog, and there are no other sources within several arc-seconds, so we consider the possibility of source confusion negligible. Using the $Gaia$ distance and PS magnitudes, we find a constraint on the donor star mass of $M_{\rm donor} \lesssim 1\,M_\odot$. Even at the 3σ upper limit on the distance $d \simeq 7.7$ kpc, the donor star is still constrained to be a main-sequence star with $M_{\rm donor} \lesssim 1.6\,M_\odot$. As such, we can confidently rule out high-mass X-ray binaries (HMXBs, $M_{\rm donor} \gtrsim 10\,M_\odot$) as potential candidates for ASASSN-18ey, although this was already unlikely because HMXBs rarely experience outbursts (Done et al. 2007).

ASAS-SN and the Asteroid Terrestrial-impact Last Alert System (ATLAS; Tonry et al. 2018) observed the location of ASASSN-18ey 403 and 707 times since 2015 January and 2015 September, respectively. ASAS-SN observes in V and g while ATLAS observes in orange (o) and cyan (c) filters. There is a bright ($V \sim 13.5$ mag) star roughly $18\overset{''}{.}0$ from ASASSN-18ey that contaminates both the ASAS-SN and ATLAS photometry in quiescence. During outburst, ASASSN-18ey is bright enough that blending is not an issue. Thus, for the pre-outburst light curve we focus on changes in flux as shown in Figure 1.

ASASSN-18ey has not had any comparable optical outbursts in the last $\sim$3.5 years. The longest interval between any two consecutive ASAS-SN or ATLAS observations is 90 days, far shorter than the current outburst which has now surpassed 150 days. Assuming a conservative ASAS-SN detection limit of 5×10^{-12} erg cm^{-2} s^{-1}, we rule out outbursts with $\gtrsim$10% of the amplitude of the current outburst since 2015 January.

The source shows noticeable variability in the pre-outburst light curve. We compute the fractional variability amplitude f (Vaughan et al. 2003) for each filter,
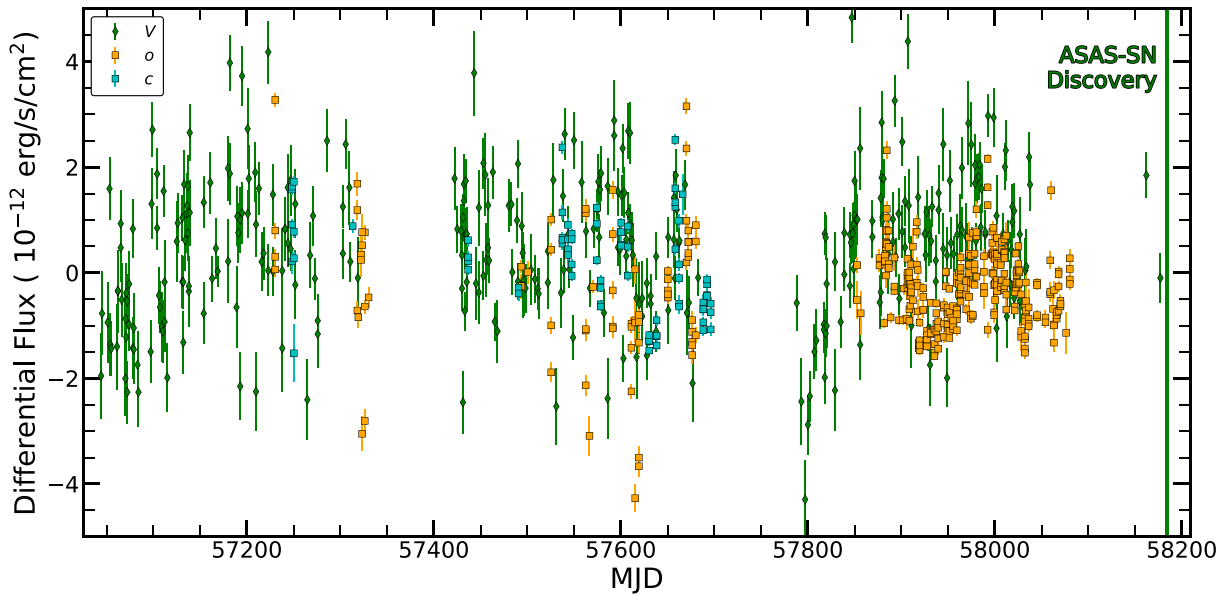
$$f_V = 0.51, \quad f_o = 0.27, \quad {\rm and} \quad f_c = 0.25 \quad ({\rm mag}),$$

much of which we attribute to intrinsic variability in ASASSN-18ey, especially given the correlations between filters. We inspected the periodograms for each light curve, but found no strong correlated peaks between them. However, cross-correlating the light curves where observations in

---

[17] http://www.astronomy.ohio-state.edu/asassn/transients.html

[18] http://archive.stsci.edu/panstarrs/stackobject/search.php
[19] http://stev.oapd.inaf.it/cgi-bin/cmd

Figure 1. Pre-outburst light curve of ASASSN-18ey from ASAS-SN and ATLAS. The green diamonds represent the ASAS-SN *V*-band, blue squares the ATLAS *c*-band, and orange squares the ATLAS *o*-band observations. There are obvious correlations between observations conducted in different filters, indicating that much of the variability is intrinsic to ASASSN-18ey and not nightly scatter. Fluxes are *not* corrected for interstellar extinction.

multiple filters are available shows that the variability is correlated, with the correlation coefficient $r \sim 0.3$–0.6, depending on the MJD range and filter choices.

Photometric variability, even in quiescence, is expected for BH LMXB systems, and is sometimes attributed to a jet (e.g., Russell et al. 2018). Some BH LMXBs have shown flux increases in the optical and near-infrared on the order of ~ 0.05 mag yr^{-1} as they approach an outburst (e.g., Bernardini et al. 2016; Russell et al. 2018). However, the ASAS-SN and ATLAS light curves are consistent with no systematic brightening since 2015.

There is a $\sim 2.4\sigma$ X-ray detection by the *ROentgen SATellite* (*ROSAT*; Pfeffermann et al. 1987) taken on MJD 48 136, almost three decades prior to the current outburst. The 373 s *ROSAT* observation has a count rate of $(4.42 \pm 3.16) \times 10^{-2}$ counts per second. Using the power-law index and $n_{\rm H}$ derived in Section 3, this corresponds to an unabsorbed flux of $(2.71 \pm 1.93) \times 10^{-12}$ erg^{-1} s^{-1} cm^{-2} in the 0.3–2 keV energy range $(L_{2–10\,{\rm keV}} \sim 10^{33}$ erg s$^{-1})$. If real, this implies an unusually high-mass transfer rate from the donor, indicating that the star has likely evolved off the main sequence. Archival photometry excludes most giant stars but subgiant stars are still possible considerations. There is also a 6 s slew-mode *XMM-Newton* observation of this location, but it provides weaker limits than those of the *ROSAT* observation.

3. Outburst and Photometric Evolution

In Figure 2 we present ASAS-SN (filters: *V*, *g*), ATLAS (filters: *o*, *c*) and *Swift Gamma-ray Burst Mission* (*Swift*; Gehrels et al. 2004) UltraViolet and Optical Telescope (UVOT, filters: *v*, *b*, *u*, *W*1, *M*2, *W*2; Roming et al. 2005), X-ray Telescope (XRT, 0.3–10 keV ; Burrows et al. 2005), and the Burst Alert Telescope (BAT, 15–50 keV; Barthelmy et al. 2005) observations covering from discovery until ~ 150 days after discovery (*Swift* PIs: Kennea, Motta, Paice, Tanaka, Altamirano, Sanchez, Yan, Markwardt, Yu, Sivakoff, and Knigge). As each UVOT epoch contained two

observations in each filter, we first combined the two images in each filter using the HEAsoft software task `uvotimsum`, and then extracted counts from the combined images in a 10″0 radius region using the software task `uvotsource`, with a sky region of $\sim 40″0$ radius used to estimate and subtract the sky background. Aperture corrections were applied to the UVOT count rates before converting into magnitudes and fluxes based on the most recent UVOT calibration (Poole et al. 2008; Breeveld et al. 2010). The brightness of ASASSN-18ey caused several *Swift b*-band observations to be saturated, as well some saturated images in other bands, which we exclude for the entirety of our analysis. The BAT data was retrieved through the BAT Transient Monitor[20] (Krimm et al. 2013) and the XRT data was retrieved through the UK *Swift* Science Data Centre[21] (Evans et al. 2007, 2009). These tools automatically handle processing steps such as source extraction and background subtraction, and mitigate potential issues such as detector pileup for bright sources.
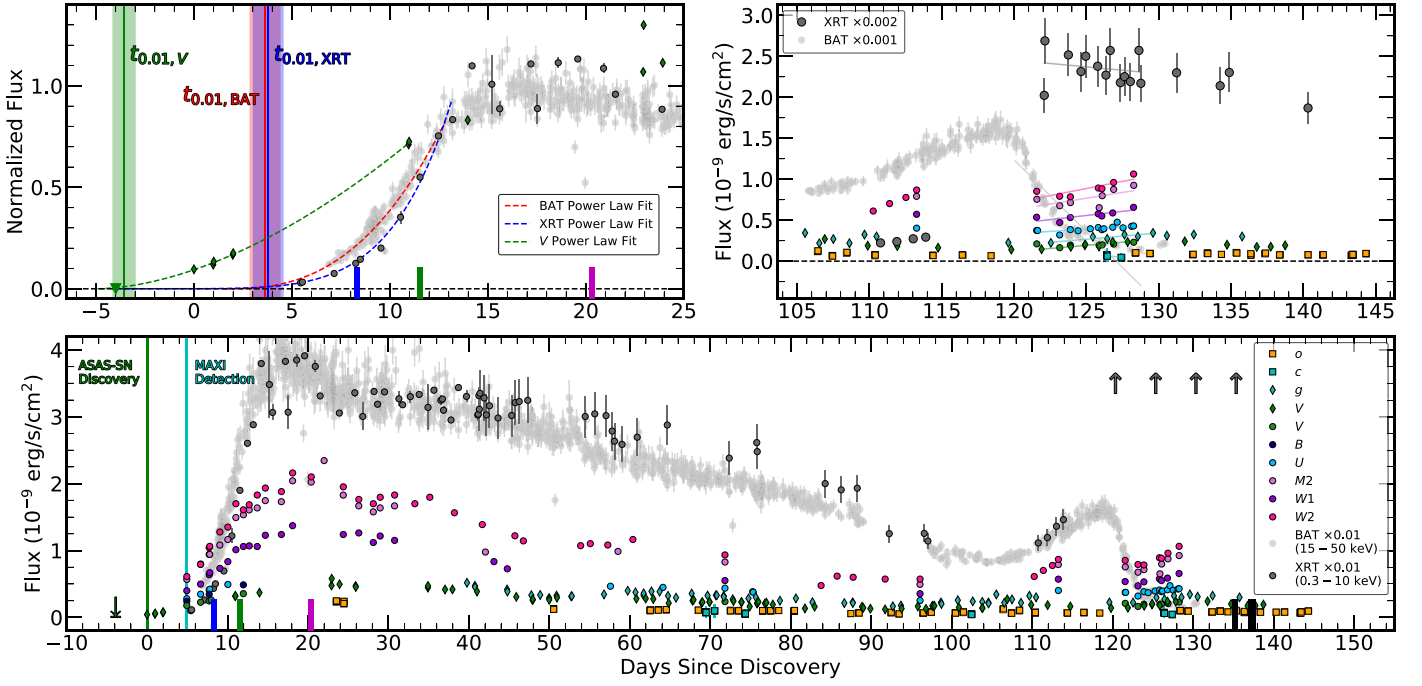
We fit the 54 XRT spectra simultaneously using XSPEC, assuming an absorbed power-law model to derive the column density along the line of sight, $N_{\rm H} = 1.05 \times 10^{21}$ cm^{-2}, and a photon index of $\Gamma = 1.4$, which we use in converting count rates to fluxes with WebPIMMS.[22] This methodology neglects the changing spectral forms of ASASSN-18ey as it undergoes the outburst, however, for our purposes, this is a sufficient treatment. This column density implies a reddening of $E(B - V) \simeq 0.18$, consistent with the estimate reported in Section 1 from Schlafly & Finkbeiner (2011). All photometry was converted to flux units (erg cm^{-2} s^{-1}) for comparison with the X-ray data and corrected for interstellar extinction/absorption. Quiescent optical fluxes, derived from the PS SOC magnitudes using conversions in Tonry et al. (2012) and Tonry et al. (2018), were added to the ASAS-SN and ATLAS

---

[20] https://swift.gsfc.nasa.gov/results/transients/
[21] http://www.swift.ac.uk/user_objects/
[22] https://heasarc.gsfc.nasa.gov/cgi-bin/Tools/w3pimms/w3pimms.pl

Figure 2. Light curves of ASASSN-18ey from discovery until ∼150 days later in the optical, UV, and X-rays. The ASAS-SN photometry is plotted as diamonds, *Swift* as circles, and ATLAS as squares. XRT and BAT X-ray light curves are scaled for visual clarity. Top left: rising light curve of ASASSN-18ey from ASAS-SN and *Swift*, including power-law fits and derived values of $t_{0.01}$ (see the text). Top right: the hard X-ray rebrightening event at ∼120 days after discovery. The optical and UV data imply a rising disk temperature (see Figure 3) even though the hard X-rays have diminished and the soft X-rays are declining, indicating a delayed response between X-ray production and the subsequent reprocessing into optical/UV emission (faint lines meant to guide the eye). The X-ray flux scales are *not* the same as in the lower panel. Bottom: full light curve of ASASSN-18ey from ASAS-SN, ATLAS, and *Swift*. At this scale, the *Swift* XRT fluxes at >120 days are off the top of the plot, as indicated by the upward arrows. The green line indicates the discovery of ASASSN-18ey and the cyan line marks the MAXI X-ray detection (Kawamuro et al. 2018). Colored ticks along the *x*-axes indicate the spectral epochs shown in Figure 4.

differential flux measurements to more accurately represent the true optical flux from ASASSN-18ey.

3.1. Rising Light Curve

The optical rises of BH LMXBs prior to the corresponding X-ray detection are generally poorly constrained, although there are a few occurrences (e.g., Orosz et al. 1997; Jain et al. 2001; Zurita et al. 2006). Similarly, ASASSN-18ey was discovered in the optical, allowing us to study its pre-X-ray transient evolution. To characterize the rising light curves we use a power law,

$$\hat{F}_\lambda(t) = A\left(\frac{t - t_{0,\lambda}}{1 \text{ day}}\right)^B, \qquad (1)$$

where $\hat{F}_\lambda$ is the normalized flux in filter λ, $t_{0,\lambda}$ is the time zero point, t is the time of the observations, and $\{A, B\}$ are coefficients. For the rising *V*-band light curve, only the ASAS-SN observations are used, as the *Swift* *v*-band is both bluer and narrower than the Johnson-Cousins *V* filters used by ASAS-SN. Since the functional form we adopt is not physically motivated and there is quiescent flux in the optical, we report the time $t_{0.01}$ at which the light curve for each filter/energy range reaches 1% of the peak flux rather than t_0. This time is closer to the data being fit and is therefore less sensitive to the exact functional form we assume.

The power-law fits to the rising ASAS-SN *V*-band, *Swift* XRT, and *Swift* BAT light curves are shown in the top left panel of Figure 2, along with the derived values of $t_{0.01}$. We use a bootstrap-resampling technique to estimate errors for the fit

parameters since the sampling of the rising light curve is sparse. The ASAS-SN *V*-band observation at ∼14 days after discovery is excluded from the fitting because it significantly reduces the quality of the fit without affecting the estimate of $t_{0.01,V}$ appreciably. For the ASAS-SN *V*-band light curve, we find $A = (5.85 \pm 2.07) \times 10^{-3}$, $B = 1.74 \pm 0.11$, and $t_{0.01,V} = -3.56 \pm 0.57$ days. For the XRT light curve, we find $A = (5.79 \pm 7.18) \times 10^{-8}$, $B = 5.82 \pm 0.35$, and $t_{0.01,XRT} = 3.80 \pm 0.77$ days. For the BAT light curve, we find $A = (1.42 \pm 1.10) \times 10^{-3}$, $B = 2.62 \pm 0.25$, and $t_{0.01,BAT} = 3.64 \pm 0.78$ days. Thus, we find a lag between the start of the optical and BAT hard X-ray outbursts of 7.20 ± 0.97 days.

We fit quadratic functions to determine the time of maximum, t_{max}, in days relative to discovery for the ASAS-SN *V*-band, XRT, and BAT light curves. We then use the derived t_{max} to calculate the flux at peak, which we use in normalizing the rising light curves. We find $t_{max} = 16.86 \pm 0.73$ days for BAT, 18.06 ± 3.99 days for XRT, and 26.20 ± 1.52 days for the ASAS-SN *V*-band. Combining these with our derived $t_{0.01}$ values, we find total rise times $t_{rise} = t_{max} - t_{0.01}$ of 13.22 ± 1.07 days, 14.26 ± 4.07 days, and 29.76 ± 1.63 days for the BAT, XRT, and the ASAS-SN *V*-band, respectively. While the optical rise begins first, the optical luminosity takes 16.54 ± 1.95 days longer to peak than the hard X-rays.

This week-long delay between the optical and X-ray flux increases is expected from DIMs and can constrain where in the disk the outburst began (Dubus et al. 2001). The outburst starts in the *V*-band at radius $R(V)$ and simultaneously propagates both inward and outward until reaching the inner regions of the disk, producing X-rays. The difference between the beginning of the optical and X-ray emission corresponds to the viscous
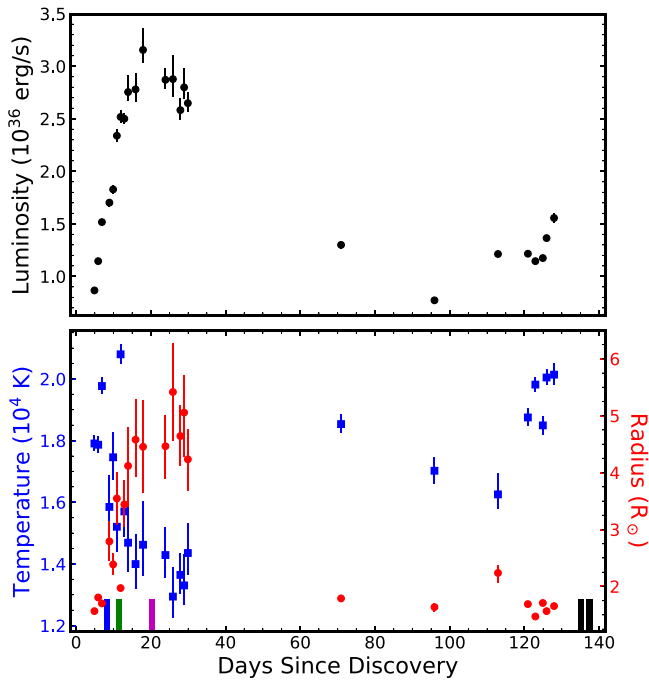
Figure 3. Luminosity (top), radius, and temperature (bottom) evolution of ASASSN-18ey from BB fits to the *Swift* photometry. Spectral epochs are shown along the bottom axis, color coded according to the spectra in Figure 4.

timescale $t_{\mathrm{visc}} = \Delta t_{V-X} = t_{0.01,V} - t_{0.01,\mathrm{BAT}}$, and constrains the location in the disk at which the outburst begins. We adopt the scaling relation of Bernardini et al. (2016), using the same parameter ranges for the hot disk viscosity parameter ($\alpha \in [0.1\text{–}0.2]$), mid-plane disk temperature ($T_s \in [3\text{–}5] \times 10^4$ K), and assumed radius of the X-ray disk ($R(X) = 5 \times 10^8$ cm). The BH mass is currently unconstrained, but the dependence is weak ($t_{\mathrm{vis}} \propto \sqrt{M_{\mathrm{BH}}/10M_\odot}$), so we assume $M_{\mathrm{BH}} \approx 8\,M_\odot$ for simplicity. Taking $t_{\mathrm{vis}} \in [6.1\text{–}8.1]$ days ($t_{\mathrm{vis}} \pm 1\sigma$), we find $R(V) = [0.8\text{–}2.5] \times 10^9$ cm $= [0.01\text{–}0.04]\,R_\odot$. This is consistent with the range found for V404 Cyg by Bernardini et al. (2016) and matches theoretical predictions for DIM+irradiation models for BH LMXB outbursts (Dubus et al. 2001).

3.2. Temperature and Photosphere Evolution

We compute the effective blackbody (BB) luminosity, temperature, and radius as a function of time for epochs with at least three *Swift* filters. An accretion disk is not usually well modeled by a simple BB and the spectral energy distribution in the observed photometry is well fit by a blackbody model, suggesting that a narrow range of temperatures dominate the peak of the emission. These BB parameters are presented in Figure 3 and errors derived using a Markov chain Monte Carlo MCMC. The overall temperature of the disk is consistent with the ionization temperature of hydrogen, as expected for an outburst driven by thermal and viscous instability (Dubus et al. 2001). The BB evolution show the photosphere to be cooling and expanding as ASASSN-18ey approaches its peak optical luminosity, consistent with an outward-propagating heating front moving through the disk.

Unfortunately, the *Swift* data has a gap from ∼35–70 days after discovery where we cannot constrain the BB evolution.

During this gap the effective temperature of the reprocessing disk increases and the photosphere recedes but we cannot constrain how quickly this change occurred.

We now have a rough picture of the structure and evolution of ASASSN-18ey as it undergoes the outburst. The initially hot and small emission region cools and expands as ASASSN-18ey reaches peak optical brightness ∼30 days after discovery. Post-peak, the photosphere shrinks and becomes hotter before starting another cooling phase. It is worth noting that this secondary cooling phase is dissimilar to the original, as the size of the emission region remains small. At the end of the linear X-ray decay, when ASASSN-18ey has settled into a quasi-static "plateau," the photosphere has reverted to a temperature and size similar to those before the peak. By ∼120 days after the peak, ASASSN-18ey has started rising in temperature, consistent with the rise in UV brightness, even as the hard X-rays turn off and the soft X-rays diminish, indicating a delayed response between X-ray production and the response of the reprocessing disk.
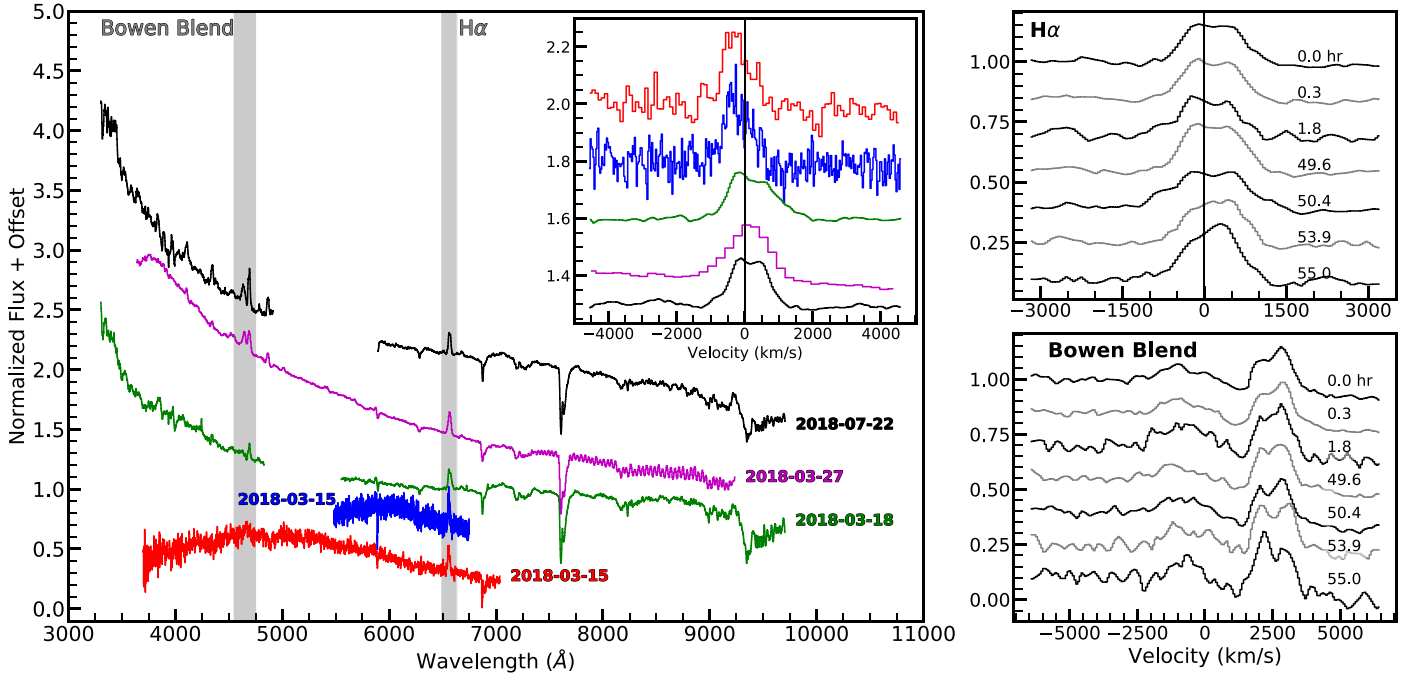
4. Spectral Evolution

In Figure 4 we show the spectroscopic evolution of ASASSN-18ey from 8 to 137 days after discovery. We present two early-time SOAR/Goodman spectra (Clemens et al. 2004) acquired roughly eight days after discovery on MJD 58192.4 taken with two separate gratings: a 600 s low-resolution spectrum spanning 3700–7000 Å and a 1200 s high-resolution spectrum spanning 5500–6800 Å. These spectra were reduced using standard IRAF routines. We also obtained one early-time (MJD 58195.6) and seven late-time (MJD 58319.3-58321.6) spectra with the University of Hawaii 88" (UH88) telescope and the SuperNova Integral Field Spectrograph (SNIFS; Lantz et al. 2004). Each spectrum was reduced with an automated pipeline and spans 3300–9700 Å excluding the dichroic crossover (∼4800–5500 Å). Finally, we supplement our spectroscopic time series with a publicly available ePESSTO (Smartt et al. 2015; Floers et al. 2018) spectrum taken near the peak.

The spectra exhibit largely featureless continua except for the Balmer lines and the Bowen blend, a forest of C III and N III lines between ∼4630–4660 Å created by high-energy irradiation of the companion star (McClintock et al. 1975). A striking feature of the spectroscopic evolution is the development of a double-peaked Hα profile (inset, Figure 4) between 8 and 11 days after discovery. Another noteworthy feature in the SNIFS pre-maximum spectrum is the appearance of a single-peaked emission line in the Bowen blend region, which becomes double-peaked ∼9 days later.

Finally, we highlight the short-timescale variations of Hα and the Bowen blend in the late-time spectra of ASASSN-18ey (right panels, Figure 4). The seven spectra, taken over 2.5 days spanning 135–137 days after discovery, exhibit shifting line profiles. Even consecutive exposures separated by <30 minutes show qualitative shifts in the Hα and Bowen blend, likely corresponding to the orbital motion of the system.

5. A New Black Hole X-Ray Binary

Figure 5 shows the location of ASASSN-18ey on the $L_X - L_{\mathrm{opt}}$ diagram from Russell et al. (2006). Due to the high-cadence optical and X-ray observations throughout the outburst, we can track the temporal evolution of ASASSN-18ey.

Figure 4. Spectroscopic evolution of ASASSN-18ey. Left: pre-maximum spectra of ASASSN-18ey (colored) and at 135 days (black). The colors correspond to those used for the colored ticks along bottom axes of Figures 2 and 3. Left inset: the region around Hα showing the broad, asymmetrical emission line that presents the first evidence of a double-peaked profile in the UH88 spectrum taken on 2018 March 18. Right panels: seven late-time (135–137 days) spectra of ASASSN-18ey zoomed into the region around Hα (top) and the Bowen blend (bottom) showing the evolving double-peaked profiles. The numbers correspond to hours after the first late-time spectrum.
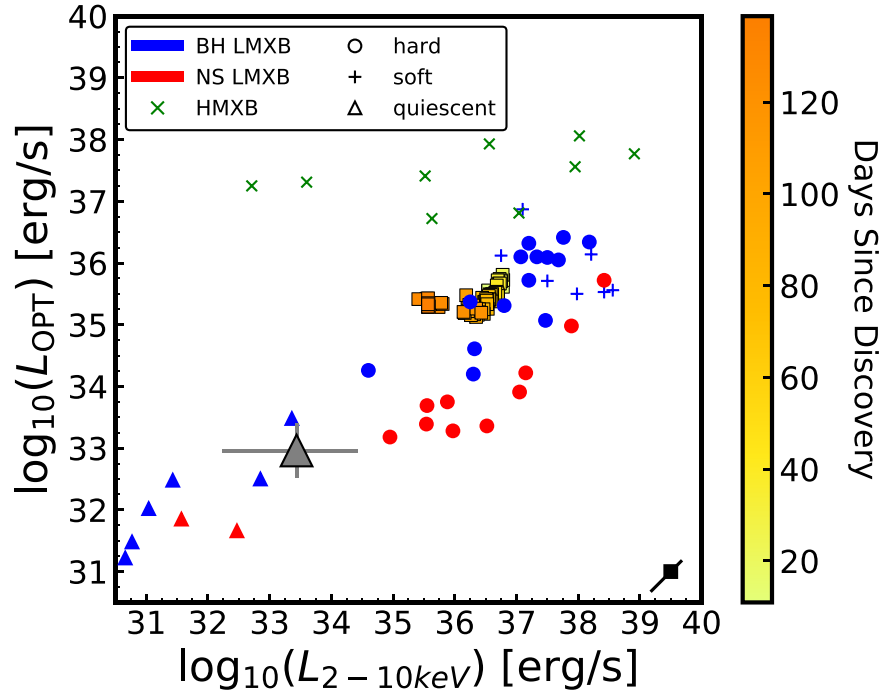
Figure 5. Evolution of ASASSN-18ey in the X-ray vs. the optical luminosity diagram along with various categories of X-ray binaries taken from Russell et al. (2006) for comparison. ASASSN-18ey coincides with the region occupied by BH LMXBs throughout the outburst. The gray triangle indicates the rough position of ASASSN-18ey assuming the pre-outburst *ROSAT* X-ray detection and optical brightness derived from PS *g*-band photometry. The black square indicates the correlated uncertainty due to the distance. The flux measurement uncertainties during outburst are negligible on this scale, and see Section 5 for an explanation of the quiescent uncertainties.

Throughout the outburst, ASASSN-18ey resides in a region occupied by BH LMXBs in the hard state. Although the pre-outburst *ROSAT* detection has low significance, the inferred X-ray luminosity and the optical luminosity agree with BH LMXBs in quiescence (Figure 5, gray triangle) The uncertainties on the quiescent X-ray flux are propagated from the low significance detection, with an additional contribution from different assumptions about the photon index of BH LMXBs in

quiescence from Remillard & McClintock (2006). The optical uncertainties stem from choosing different filters from the archival PS SOC photometry to calculate the quiescent luminosity (see Section 2).

ASASSN-18ey is almost certainly a new BH LMXB. The pre-outburst optical light curve is intrinsically variable, consistent with an unstable accretion system. The quiescent X-ray and optical fluxes preclude HMXBs, persistent NS LMXBs, and all giant companions. An outburst of $\Delta V \sim 6$ mag matches known BH LMXB outbursts (Corral-Santana et al. 2016) and precludes most non-BH systems where the accretion disks are less likely to be unstable and thus less likely to experience an outburst (Done et al. 2007). The peak of the soft and hard X-ray light curves precedes the UV, which in turn precedes the optical peaks, providing further evidence of an accretion disk that is reprocessing the accretion-generated X-rays and increasing in temperature. Veledina et al. (2018) conducted polarimetric observations of ASASSN-18ey in outburst, finding only a minimal amount of polarized flux ($<1\%$), consistent with the majority of optical flux stemming from the disk. The temperature of the disk ($\sim 10^4$ K) and ~ 7 day delay between the optical and X-ray rise are consistent with an outburst driven by H ionization instability. The spectra show typical characteristics of LMXBs in outburst, such as variable Hα and Bowen blend profiles. The evolution of ASASSN-18ey on the $L_X - L_{\rm opt}$ diagram during the outburst further strengthens the classification as a new BH X-ray binary, as it resides in a region dominated by BH LMXBs for the entirety of the outburst.

Once the system has returned to quiescence and the mass of the BH is determined, we can use $t_{\rm vis}$ to constrain, rather than assume, the temperature and viscosity of the hot disk at the beginning of the outburst. This demonstrates the benefit of catching BH LMXBs outbursts on the rise. ASASSN-18ey has the potential to be the best-studied BH LMXB outburst to date, with more than 40 Astronomer's Telegrams and $>360,000$ observations from 50 observers reported on the AAVSO Light Curve Generator[23] as of 2018 October 1 (Kafka 2018).

ORCID iDs

M. A. Tucker ⬤ https://orcid.org/0000-0002-2471-8442
K. Auchettl ⬤ https://orcid.org/0000-0002-4449-9152
J. Strader ⬤ https://orcid.org/0000-0002-1468-9668
C. S. Kochanek ⬤ https://orcid.org/0000-0001-6017-2961
A. Bahramian ⬤ https://orcid.org/0000-0003-2506-6041
John F. Beacom ⬤ https://orcid.org/0000-0002-0005-2631
L. Chomiuk ⬤ https://orcid.org/0000-0002-8400-3705
H. Flewelling ⬤ https://orcid.org/0000-0002-1050-4056
A. N. Heinze ⬤ https://orcid.org/0000-0003-3313-4921
B. Stalder ⬤ https://orcid.org/0000-0003-0973-4900
M. E. Huber ⬤ https://orcid.org/0000-0003-1059-9603
D. M. Rowan ⬤ https://orcid.org/0000-0003-2431-981X
K. Dage ⬤ https://orcid.org/0000-0002-8532-4025

References

Baglio, M. C., Russell, D. M., & Lewis, F. 2018, ATel, 11418, 1
Bahramian, A., Strader, J., & Dage, K. 2018, ATel, 11424, 1
Bailer-Jones, C. A. L., Rybizki, J., Fouesneau, M., Mantelet, G., & Andrae, R. 2018, arXiv:1804.10121
Barthelmy, S. D., Barbier, L. M., Cummings, J. R., et al. 2005, SSRv, 120, 143
Berdyugin, A., Veledina, A., Kosenkov, I., et al. 2018, ATel, 11445, 1
Bernardini, F., Russell, D. M., Shaw, A. W., et al. 2016, ApJ, 818, L5
Bozzo, E., Savchenko, V., Ferrigno, C., et al. 2018, ATel, 11478, 1
Breeveld, A. A., Curran, P. A., Hoversten, E. A., et al. 2010, MNRAS, 406, 1687
Bright, J., Fender, R., & Motta, S. 2018a, ATel, 11420, 1
Bright, J., Motta, S., Fender, R., Perrott, Y., & Titterington, D. 2018b, ATel, 11827, 1
Broderick, J., Bright, J., Russell, T., et al. 2018a, ATel, 11609, 1
Broderick, J., Russell, T., Bright, J., et al. 2018b, ATel, 11887, 1
Buisson, D., Fabian, A., Alston, W., et al. 2018, ATel, 11578, 1
Burrows, D. N., Hill, J. E., Nousek, J. A., et al. 2005, SSRv, 120, 165
Casella, P., Vincentelli, F., O'Brien, K., et al. 2018, ATel, 11451, 1
Chambers, K. C., Magnier, E. A., Metcalfe, N., et al. 2016, arXiv:1612.05560
Clemens, J. C., Crain, J. A., & Anderson, R. 2004, Proc. SPIE, 5492, 331
Corral-Santana, J. M., Casares, J., Muñoz-Darias, T., et al. 2016, A&A, 587, A61
Del Santo, M., & Segreto, A. 2018, ATel, 11427, 1
Denisenko, D. 2018, ATel, 11400, 1
Done, C., Gierliński, M., & Kubota, A. 2007, A&ARv, 15, 1
Dubus, G., Hameury, J. M., & Lasota, J. P. 2001, A&A, 373, 251
Evans, P. A., Beardmore, A. P., Page, K. L., et al. 2007, A&A, 469, 379
Evans, P. A., Beardmore, A. P., Page, K. L., et al. 2009, MNRAS, 397, 1177

---

[23] https://www.aavso.org/lcg

Fiori, M., Zampieri, L., Burtovoi, A., et al. 2018, ATel, 11824, 1
Flewelling, H. A., Magnier, E. A., Chambers, K. C., et al. 2016, arXiv:1612.05243
Floers, A., Taubenberger, S., Vogl, C., et al. 2018, ATel, 11480, 1
Gaia Collaboration, Brown, A. G. A., Vallenari, A., et al. 2018, arXiv:1804.09365
Gaia Collaboration, Prusti, T., de Bruijne, J. H. J., et al. 2016, A&A, 595, A1
Gandhi, P., Paice, J. A., Littlefair, S. P., et al. 2018, ATel, 11437, 1
Garnavich, P., & Littlefield, C. 2018, ATel, 11425, 1
Gehrels, N., Chincarini, G., Giommi, P., et al. 2004, ApJ, 611, 1005
Homan, J., Altamirano, D., Arzoumanian, Z., et al. 2018a, ATel, 11576, 1
Homan, J., Uttley, P., Gendreau, K., et al. 2018b, ATel, 11820, 1
Homan, J., Uttley, P., Gendreau, K., et al. 2018c, ATel, 11823, 1
Jain, R. K., Bailyn, C. D., Orosz, J. A., McClintock, J. E., & Remillard, R. A. 2001, ApJ, 554, L181
Kafka, S. 2018, Observations from the AAVSO International Database, https://www.aavso.org
Kawamuro, T., Negoro, H., Yoneyama, T., et al. 2018, ATel, 11399, 1
Kennea, J. A., Marshall, F. E., Page, K. L., et al. 2018, ATel, 11403, 1
Kochanek, C. S., Shappee, B. J., Stanek, K. Z., et al. 2017, PASP, 129, 104502
Krimm, H. A., Holland, S. T., Corbet, R. H. D., et al. 2013, ApJS, 209, 14
Kuulkers, E., Bozzo, E., Ferrigno, C., Belloni, T., & Sanchez-Fernandez, C. 2018, ATel, 11490, 1
Lantz, B., Aldering, G., Antilogus, P., et al. 2004, Proc. SPIE, 5249, 146
Lasota, J.-P. 2001, NewAR, 45, 449
Littlefield, C. 2018, ATel, 11421, 1
Luri, X., Brown, A. G. A., Sarro, L. M., et al. 2018, arXiv:1804.09376
Mandal, A. K., Singh, A., Stalin, C. S., Chandra, S., & Gandhi, P. 2018, ATel, 11458, 1
Marigo, P., Girardi, L., Bressan, A., et al. 2017, ApJ, 835, 77
Matsuoka, M., Kawasaki, K., Ueno, S., et al. 2009, PASJ, 61, 999
McClintock, J. E., Canizares, C. R., & Tarter, C. B. 1975, ApJ, 198, 641
Mereminskiy, I. A., Grebenev, S. A., Molkov, S. V., et al. 2018, ATel, 11488, 1
Mihara, T., Nakajima, M., Sugizaki, M., et al. 2011, PASJ, 63, S623
Munoz-Darias, T., Jimenez-Ibarra, F., Padilla, M. A., Casares, J., & Torres, M. A. P. 2018, ATel, 11481, 1

Orosz, J. A., Remillard, R. A., Bailyn, C. D., & McClintock, J. E. 1997, ApJL, 478, L83
Paice, J. A., Gandhi, P., Page, K., et al. 2018, ATel, 11432, 1
Pfeffermann, E., Briel, U. G., Hippmann, H., et al. 1987, Proc. SPIE, 733, 519
Polisensky, E., Giacintucci, S., Peters, W. M., Clarke, T. E., & Kassim, N. E. 2018, ATel, 11540, 1
Poole, T. S., Breeveld, A. A., Page, M. J., et al. 2008, MNRAS, 383, 627
Remillard, R. A., & McClintock, J. E. 2006, ARA&A, 44, 49
Richmond, M. 2018, ATel, 11596, 1
Roming, P. W. A., Kennedy, T. E., Mason, K. O., et al. 2005, SSRv, 120, 95
Russell, D. M., Fender, R. P., Hynes, R. I., et al. 2006, MNRAS, 371, 1334
Russell, D. M., Qasim, A. A., Bernardini, F., et al. 2018, ApJ, 852, 90
Sako, S., Ohsawa, R., Ichiki, M., et al. 2018, ATel, 11426, 1
Schlafly, E. F., & Finkbeiner, D. P. 2011, ApJ, 737, 103
Shappee, B. J., Prieto, J. L., Grupe, D., et al. 2014, ApJ, 788, 48
Smartt, S. J., Valenti, S., Fraser, M., et al. 2015, A&A, 579, A40
Tetarenko, A. J., Bremer, M., Bright, J., et al. 2018a, ATel, 11440, 1
Tetarenko, A. J., Petitpas, G., Sivakoff, G. R., et al. 2018b, ATel, 11831, 1
Tonry, J. L., Denneau, L., Heinze, A. N., et al. 2018, PASP, 130, 064505
Tonry, J. L., Stubbs, C. W., Lykke, K. R., et al. 2012, ApJ, 750, 99
Townsend, A., Jeram, S., Eikenberry, S., et al. 2018, ATel, 11574, 1
Trushkin, S. A., Nizhelskij, N. A., Tsybulev, P. G., & Erkenov, A. 2018a, ATel, 11439, 1
Trushkin, S. A., Nizhelskij, N. A., Tsybulev, P. G., & Erkenov, A. 2018b, ATel, 11539, 1
Uttley, P., Gendreau, K., Markwardt, C., et al. 2018, ATel, 11423, 1
Vaughan, S., Edelson, R., Warwick, R. S., & Uttley, P. 2003, MNRAS, 345, 1271
Veledina, A., Berdyugin, A. V., Kosenkov, I. A., et al. 2018, arXiv:1808.09002
Yamanaka, M., Nakaoka, T., Kawabata, M., et al. 2018, ATel, 11855, 1
Yu, W., Zhang, J., Yan, Z., Wang, X., & Bai, J. 2018a, ATel, 11510, 1
Yu, W., Lin, J., Mao, D., et al. 2018b, ATel, 11591, 1
Zampieri, L., Fiori, M., Burtovoi, A., et al. 2018, ATel, 11723, 1
Zurita, C., Torres, M. A. P., Steeghs, D., et al. 2006, ApJ, 644, 432